NUMERICAL SIMULATIONS OF COUNTER-CURRENT TWO-PHASE FLOW EXPERIMENTS IN A PWR HOT LEG MODEL USING AN INTERFACIAL AREA DENSITY MODEL

Thomas Höhne, Deendarlianto, Christophe Vallée, Dirk Lucas and Matthias Beyer

Helmholtz-Zentrum Dresden-Rossendorf (HZDR), Institute of Safety Research, P.O. Box 510 119, D-01314 Dresden, Germany.

Email: t.hoehne@hzdr.de

Abstract

In order to improve the understanding of counter-current two-phase flows and to validate new physical models, CFD simulations of 1/3rd scale model of the hot leg of a German Konvoi PWR with rectangular cross section was performed. Selected counter-current flow limitation (CCFL) experiments at the Helmholtz-Zentrum Dresden-Rossendorf (HZDR) were calculated with ANSYS CFX 12.1 using the multi-fluid Euler-Euler modeling approach. The transient calculations were carried out using a gas/liquid inhomogeneous multiphase flow model coupled with a SST turbulence model for each phase. In the simulation, the surface drag was approached by a new correlation inside the Algebraic Interfacial Area Density (AIAD) model. The AIAD model allows the detection of the morphological form of the two phase flow and the corresponding switching via a blending function of each correlation from one object pair to another. As a result this model can distinguish between bubbles, droplets and the free surface using the local liquid phase volume fraction value. A comparison with the high-speed video observations shows a good qualitative agreement. The results indicated that quantitative agreement of the CCFL characteristics between calculation and experimental data was obtained. The goal is to provide an easy usable AIAD framework for all ANSYS CFX users, with the possibility of the implementation of their own correlations.

Keywords: Numerical simulation, CFD, CCFL, AIAD model, reflux condensation, PWR hot leg, air-water experiment

1. INTRODUCTION

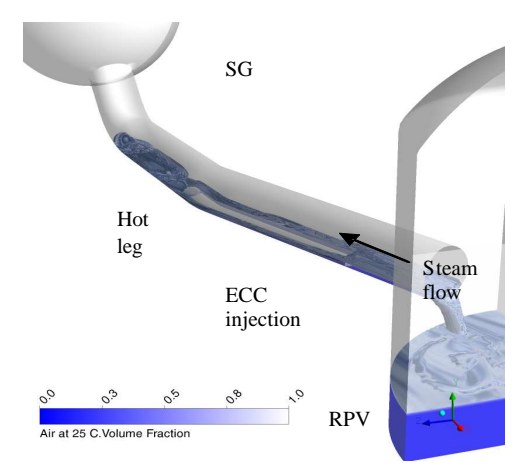


Fig. 1 Counter-current gas-liquid two-phase flow in PWR Hot leg

The counter-current gas-liquid two-phase flow in the hot leg of a pressurized water reactor (PWR) has received special attention in nuclear reactor safety research.

In the event of a loss-of-coolant-accident (LOCA) in a pressurized water reactor (PWR), emergency strategies have to be mapped out in order to guarantee a safe removal of the decay heat from the reactor core - also in case of a component breakdown. During a hypothetical small break LOCA with failure of the high pressure emergency core cooling system (ECC) and of the main feed pumps, a natural circulation starts in the primary circuit. This allows the heat removal, also if steam is generated in the reactor core due to the depressurization of the primary circuit. But if during the further run, the water level in the reactor pressure vessel (RPV) falls below the hot-leg inlet, only steam will flow to the steam generator. Therefore, the natural circulation breaks down and switches to the reflux condenser mode.

In the reflux condenser mode, the steam coming from the RPV condenses in the vertical U-tubes of the steam generator. In each half of the steam generator, the condensate flows down the tube in which it has been formed. Therefore, about one half of the condensate flows as usual over the pump to the downcomer, whereas the other half flows over the hot-leg back to the upper plenum. In the hot-leg, the condensate has to flow in counter-current to the steam.

The horizontal stratified counter-current flow of condensate and steam is only stable for a certain range of flow rates. If the steam flow increases too much, the condensate is clogged in the hot-leg. This is the beginning of the counter-current flow limitation (CCFL): the liquid is deflected by the steam and partially entrained in opposite direction to the steam generator. As a consequence, the hot-leg and the steam generator are flooded, this decreases the water level in the RPV and reduces the core cooling. In case of an additional increase of the steam flow, the condensate is completely blocked and the cooling of the reactor core from the hot-leg is impossible. The detailed examples of such LOCA scenarios leading to the reflux condenser mode can be found in Jeong (2002).

The flow conditions governing the reflux condenser mode or the counter-current flow limitation cannot be predicted with the required accuracy and spatial resolution by the state of the art one-dimensional system codes. In order to improve the modeling of these flow regimes, computational fluid dynamics (CFD) codes are currently under development. In CFD, closure models are required that must be validated, especially if they are to be applied to reactor safety issues. The aim of our experimental investigations of stratified two-phase flows is mainly to deliver high resolution data that is needed for the validation of CFD codes. In order to improve the transient analysis of counter-current two-phase flows, a $1/3^{\rm rd}$ scale model of the hot leg PWR of a German Konvoi Pressurized Water Reactor with rectangular cross section was used at Helmholtz-Zentrum Dresden-Rossendorf (HZDR) to perform experiments related to CCFL flow regimes (Vallée et al. 2009).

The widely used analysis to model the counter-current flow limitation is reported by Ardron & Banerjee (1986), Bertadano (1994) and Wongwises (1996).

Wang & Mayinger (1995) simulated two-dimensional analysis of counter-current model of UPTF Test A2 & Test 11 using a two-fluid model. They implemented the interfacial friction factor proposed by Lee & Bankoff (1983) and Ohnuki (1986) into the CFD code FLOW3D. They reported that satisfactory results were obtained, whereas, under the reflux condensation conditions, numerical computation reveals that different flow structures appeared in the region away from CCFL line and in the region near the CCFL line. Next, Minami et al. (2009) and Murase et al. (2009) conducted a three dimensional CFD simulation on the counter-current gas-liquid flow in a PWR hot-leg airwater flow in a 1/15th scale model. They used the Volume of Fluid (VOF) model and Euler- Euler on the CFD code FLUENT. In their simulations, the interfacial friction factors were adopted from the empirical correlations obtained from literatures for the cases of annular and slug flow. Those correlations were obtained on the basis of one dimensional analysis.

This paper further provides post-test CFD calculations of the air-water respectively steam-water CCFL experiments at the TOPFLOW Hot Leg model. The aim of this simulation is the validation of prediction of CCFL in a model hot leg PWR with newly developed and implemented multiphase flow models in the code ANSYS CFX. The Algebraic Interfacial Area Density (AIAD) model (Höhne, 2010) was used, which allows the detection of the morphological form of the two phase flow and the corresponding switching via a blending function of each correlation from one object pair to another. The new drag correlation obtained from this model considered the 3D effects of the simulated phenomenon.

2. THE HOT LEG MODEL OF TOPFLOW

The details of the experimental apparatus and procedure used in the present study were described in the previous papers (Deendarlianto et al., 2008 & Vallée et al. 2009) and only the main features are presented here. Fig. 2 shows a photo of the experimental facility. Fig. 3 shows a schematic diagram of the CCFL counter current flow experiments. Two vessels simulate the reactor pressure vessel (RPV) simulator and steam generator (SG) separator. They are connected by a test section that simulates the $1/3^{rd}$ scale model of the hot leg PWR of a German Konvoi Pressurized Water Reactor. Both the RPV simulator and SG separator are identical vessels with $0.8 \text{ m} \times 0.5 \text{ m} \times 1.55 \text{ m}$ ($D \times W \times H$) cubic shape. The water levels in both vessels were determined by the measurement of the differential

pressure between the top and the bottom of the vessels with differential pressure transducers. A vortex meter was used to measure the injected water mass flow rate. The injected air mass flow rate was measured and controlled using thermal mass flow meters.



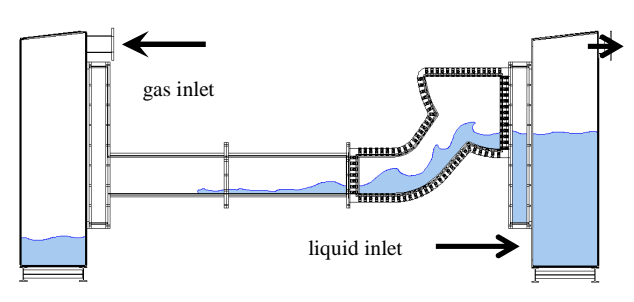


Fig. 2: TOPFLOW Hot leg model in front of the Fig. 3: Schematic diagram of the CCFL counter current pressure chamber flow experiments

The test section is composed of a horizontal rectangular channel, a bend that connects it to an upward inclined and expended channel, and a quarter of a circle representing the steam generator inlet chamber. The horizontal part of test section is 2.12 m long and has a rectangular cross-section of 0.05 m $\times 0.25$ m. The riser is 0.23 m long, has an inclination of 50° to the horizontal plane and an expansion angle of 7.5° . The inner and outer bend radii of curvature were 0.25 and 0.5 m, respectively. The test section was made of stainless steel and was equipped with glass windows to allow visual observation. The flow behavior was recorded by a high-speed video camera at frequencies of 60– 100 Hz and a shutter speed of 1/1000 s.

In the experiment, a constant water flow rate was injected at the bottom of the SG simulator from where it can flow through the test section to the RPV simulator. The gas was injected into the RPV simulator from the top and flowed through the test section in counter-current to the water flow to the SG separator (Fig. 3). The increase of the water level in the RPV simulator was used to determine the water flow rate streaming over the test section (discharge flow). The onset of flooding was defined as the limiting point of stability of the counter-current flow, indicated by the maximum air mass flow rate at which the down-flowing water mass flow rate is equal to the inlet water mass flow rate.

This experimental apparatus is put in a pressure chamber, where it was operated in pressure equilibrium with the inner atmosphere of the tank. A compressor system allows an increase of the air pressure in the chamber to a maximum of 5 MPa, which is also the maximum operation pressure of the hot leg model. The detailed principle of the pressure equilibrium technique was described by Prasser et al. (2006).

3. COMPUTATIONAL MODELLING

3.1 Free Surface Modeling

The CFD simulation of free surface flows can be performed using the multi-fluid Euler-Euler modeling approach available in ANSYS CFX. Detailed derivation of the two-fluid model can be found in the book of Ishii and Hibiki (2006). However, it requires careful treatment of several aspects of the model:

- o The interfacial area density should satisfy the integral volume balance condition. In the case of when surface waves are present, their contribution to the interfacial area density should be taken into account.
- The turbulence model should address the damping of turbulence near the free surface.
- The interphase momentum models should take into account the surface morphology.

In the present simulation, the conservation and momentum equations of the two-fluid model are solved, which have the following form

$$\frac{\partial (r_k \rho_k)}{\partial t} + \nabla (r_k \rho_k U_k) = 0 \tag{1}$$

$$\frac{\partial (r_k \rho_k)}{\partial t} + \nabla (r_k \rho_k U_k U_k) = -r_k \nabla p_k + r_k \rho_k g + \nabla r_k (\tau^{\nu} + \tau_k^t) + \tau_D$$
(2)

where the subscript k denotes phase gas or liquid, ρ is the density, u is the velocity vector, t is the time, p is the pressure, g is the gravitational acceleration, r is the volume fraction, τ is the shear stress (τ ' is the average viscous shear stress, τ ' is the turbulent shear stress) and τ_D is the interfacial shear stress.

In slug flow simulations, the air bubble in the water can be resulted by the drag force. The total drag force is derived from the interfacial shear stress ($F_D = \tau_D$.A), is most conveniently expressed in terms of the dimensionless drag coefficient C_D

$$F_D = C_D A \rho_{IG} |(U_L - U_G)|^2$$
(3)

where ρ_{LG} is the average density, $|(U_{_L} - U_{_G})|$ is the relative velocity and A is the projected area of the body in flow direction (interfacial area density).

3.2 The Algebraic Interfacial Area Density (AIAD) Model

Fig. 4 shows different morphologies at slug flow conditions. Separate models are necessary for dispersed particles and separated continuous phases (interfacial drag etc.). Two approaches are possible within the Euler-Euler methodology:

- Four phases: Bubble/Droplet generation and degassing have to be implemented as sources and sinks
- Two phases: Momentum exchange coefficients depend on local morphology

For the second approach Egorov (2004) proposed an Algebraic Interfacial Area Density (AIAD) Model. The basic idea of the model is:

- The interfacial area density allows the detection of the morphological form and the corresponding switching of each correlation from one object pair to another.
- It provides a law for the interfacial area density and the drag coefficient for full range 0≤r≤1.
- The model improves the physical modeling in the asymptotic limits of bubbly and droplet flows.

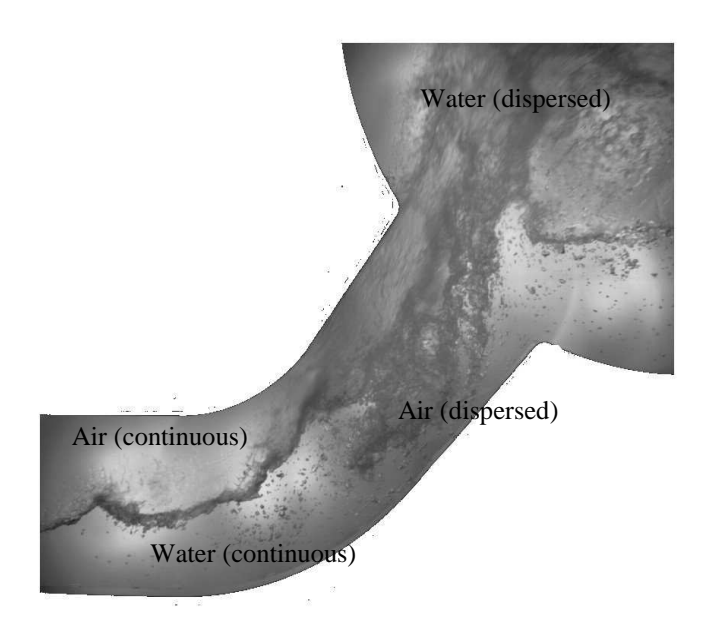


Fig.4: Different morphologies under slug flow conditions

o The interfacial area density in the intermediate range is set to the interfacial area density for free surface

The AIAD model applies three different drag coefficients, $C_{D,B}$ for bubbles, $C_{D,D}$ for the droplets and $C_{D,FS}$ for free surface. Non-drag forces (e.g. lift force and turbulent dispersion force) are neglected at the moment. The interfacial area density A also depends on the morphology of the phases. For bubbles it is

$$A = \frac{6r_G}{d_R} \tag{4}$$

where the interface area density is equal to the surface area of the spheres of diameter d_B , which occupy the gas volume fraction r_G .

For a free surface an important requirement for the model is the normalizing condition: the volume integral of the area density must be equal to the real surface area. It means that integration of the area density along a normal to the surface must yield unity:

$$\int_{-\infty}^{+\infty} A \, dn = 1 \tag{5}$$

A model, which satisfies this condition, calculates the interface area density as the absolute value of the volume fraction gradient:

$$A_{FS} = \left| \nabla r_L \right| = \frac{\partial r_L}{\partial n} \tag{6}$$

if n is directed to the bulk liquid phase. For ρ the average density is applied, i.e.

$$\rho = r_G \rho_G + r_L \rho_L \tag{7}$$

where r_L and r_G are the liquid and the gas phase density respectively. In the bubbly regime, where a_G is low, the average density ρ is close to the liquid phase density ρ_L . According to the flow regime (bubbly flow, droplet flow or stratified flow with a free surface) the corresponding drag coefficients and interfacial area densities have to be applied.

The simplest switching procedure for the interfacial area density, uses the blending function f_D . Introducing void fraction limits, the weights for flow regimes and length scales for bubbly and droplet flow (d_B, d_D) are the following:

$$f_D = \left[1 + e^{a_D(r_L - r_{D,Limit})}\right] \tag{8}$$

$$f_B = \left[1 + e^{a_B(r_G - r_{B,Limit})} \right] \tag{9}$$

$$f_{FS} = 1 - f_B - f_D \tag{10}$$

$$A = f_{FS}A_{FS} + f_BA_B + f_DA_D \tag{11}$$

$$C_D = f_{FS}C_{DFS} + f_BC_{DB} + f_DC_{DD}$$
 (12)

After a validation study for the simulation of slug flow the void fraction limits of $r_{B,limit}$ =0.3 resp. $r_{D,limit}$ =0.3 and blending coefficients of a_B = a_D =70 were used.

3.3 Modeling the free surface drag

In simulations of free surface flows eq. (3) does not represent a realistic physical model. It is reasonable to expect that the velocities of both fluids in the vicinity of the interface are rather similar. To achieve this result, a shear stress like a wall shear stress is assumed near the surface from both sides to reduce the velocity differences of both phases.

A viscous fluid moving along a "solid" like boundary will incur a shear stress, the no-slip condition, the morphology region "free surface" is the boundary layer, the shear stress is imparted onto the boundary as a result of this loss of velocity

$$\tau_{w} = \mu \frac{\partial u}{\partial y} \Big|_{y=0} \tag{13}$$

The components of the Normal vector at the free surface are taken from the gradients of the void fraction in x,y,z directions. To use these directions of the normal vectors the gradients of gas/liquid velocities which are used to calculate the wall shear stress onto the free surface are weighted with the absolute value of components of the normal vector:

$$\tau_{L,G} = \mu_{L,G} \sqrt{\frac{\partial u_{x,L,G}}{\partial x} \cdot \frac{\left(\frac{\partial r_{L,G}}{\partial x}\right)^{2}}{A_{FS}}} + \left(\frac{\partial u_{y,L,G}}{\partial y} \cdot \frac{\left(\frac{\partial r_{L,G}}{\partial y}\right)}{A_{FS}}\right)^{2} + \left(\frac{\partial u_{z,L,G}}{\partial z} \cdot \frac{\left(\frac{\partial r_{L,G}}{\partial z}\right)}{A_{FS}}\right)^{2}}$$
(14)

As a result the modified drag coefficient is dependent on the viscosities of both phases, the local gradients of gas/liquid velocities normal to the free surface, the liquid density and the slip velocity between the phases:

$$C_D = \frac{2\left[r_L \tau_{W,L} + r_G \tau_{W,G}\right]}{\rho_L \cdot U^2} \tag{15}$$

3.4 Numerical Setup & Boundary Conditions

The gas/liquid CCFL phenomenon in the hot-leg model was calculated with Euler-Euler inhomogeneous mixture model using ANSYS CFX 12.1. ANSYS CFX-12 is an element-based finite-volume method with second-order discretization schemes in space and time. It uses a coupled algebraic multigrid algorithm to solve the linear systems arising from discretization. The discretization schemes and the multigrid solver are scalably parallelized. CFX-12 works with unstructured hybrid grids consisting of tetrahedral, hexahedral, prism and pyramid elements. The calculation model is shown in Fig. 5.

TD 1 1	4	α 1	1	
Table.		1 0 0	110t101	ring
Taine.		Calci	паног	i i uns

Exp. Run	m_L [kg/s]	m_G [kg/s]	System pressure [MPa]
30-05 (Air-water)	0.307	max. 0.251	0.305
30-09 (Air-water)	0.3	0.183-0.274	0.15
11-01 (Steam-water)	0.3	0.490-0.6690	1.50

In CFD analysis, demonstration of grid independence is a basic requirement as indicated in The ERCOFTAC Best Practice Guidelines (2001), which were specified for nuclear reactor safety calculations within the ECORA project (Menter, 2002). In the present simulations, very carefully developed structured mesh for most of the flow field was adequate, at which the local refinement on them were carried out. Here, the effect of numerical diffusion can be minimized by using meshes with a finer resolution, higher order discretization methods and suitable time step sizes. As a result, a structured mesh consisted of 248,610 hexahedral elements and 281,076 nodes.

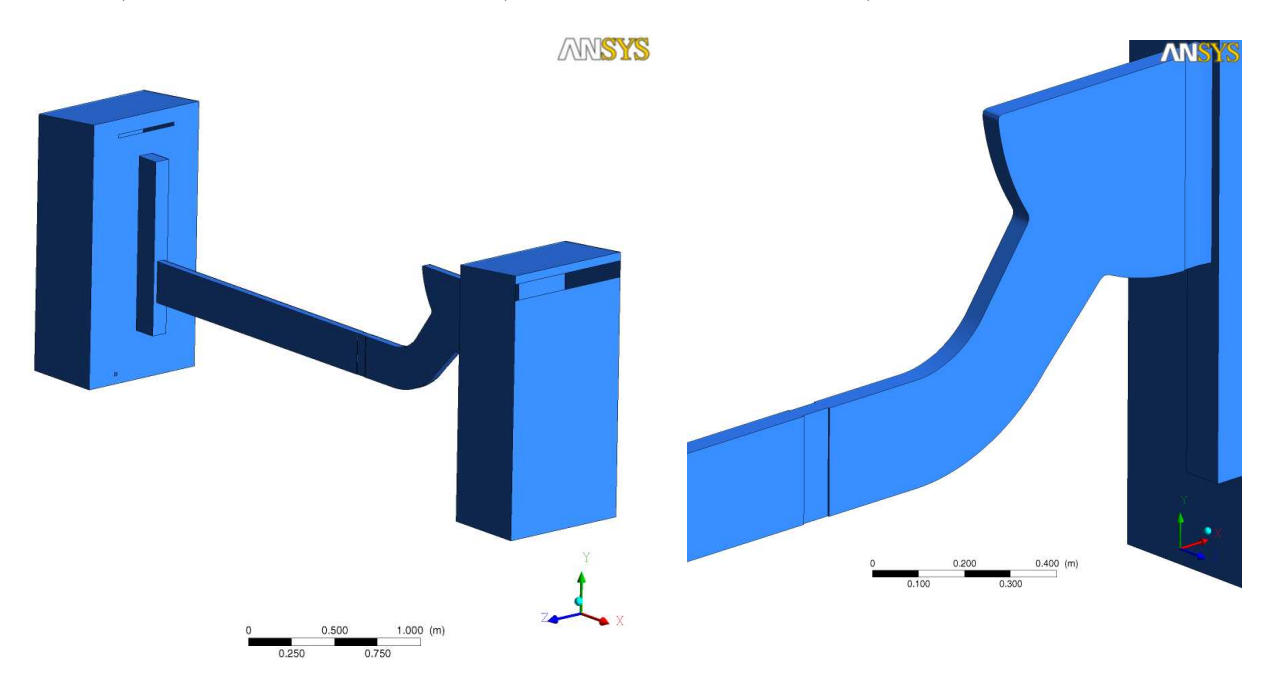


Fig. 5 Calculation domain

Three calculations have been performed of two HZDR experimental run (30-05, 30-09 and 11-01), and they are summarized in Table 1. The injected gas mass flow rates used in the present calculation were a function of time as shown in Fig. 7 and Fig. 13.

The Shear Stress Transport (SST) turbulence model was used. The SST model works by solving a turbulence/frequency-based model (k– ω) at the wall and standard k– ω in the bulk flow. A blending function ensures a smooth transition between those two models (Menter, 1993).

Both phases have treated as isothermal and incompressible. Buoyancy effects between the two-phase were taken into account by the direction of gravity term. The turbulence properties at the inlet of air and water were set using the "turbulence intensity of 5% in both phases". The air outlet was modeled with an opening boundary condition. The inner surface of the channel walls has been defined as hydraulically smooth with a non-slip boundary condition applied to both gas and liquid phases. The Drag coefficient, C_D , was determined by the AIAD model (Eq. (15), and its implementation into CFX was done via the command language CCL (CFX expression language). The calculations

were performed in parallel of 4 processors of HZDR Linux cluster. Typical computation time for each case was about 4 months.

4. RESULTS & DISCUSSIONS

The simulation for the experiment 30-05 (see Table 1) has focused primarily on the comparison of typical flow processes and code validation. Further simulations for the tests 30-09 (air-water) and 11-01 (steam-water) were used to test the ability of the AIAD model in CFX model to predict the flooding curve. CFD studies without using the AIAD model and using a uniform C_D have showed, that CCFL phenomena could not be predicted.

4.1 Air-Water-CCFL Experiment 30-05

The initial conditions of the calculation are shown in Fig. 6. Here the water is modeled at the SG simulator bottom and flows in the direction of RPV simulator. There, the water level is lower than in the channel. Moreover, the figure shows the hydrostatic pressure in the water phase.

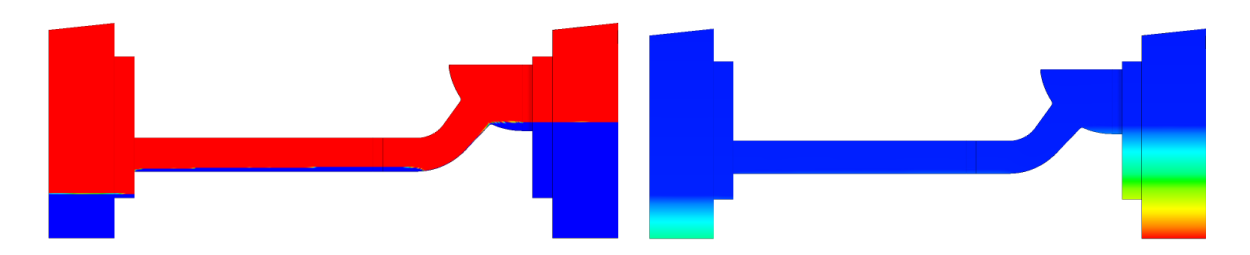


Fig. 6 Water level initial condition: Overflow elbow (left), hydrostatic pressure in the water phase (right)

The measurement data of the air mass flow of the experiment in Fig. 7 at the camera time position (yellow labels) were used as boundary conditions for the CFD calculation.

Fig. 8 shows snapshots of the time course of development of the flow. First, the water can still flow freely to the RPV simulator (Fig. 8a). As in this experiment, a hydraulic jump is observed below the elbow (see also Fig. 9). After increasing the air mass flow a partial counter-current flow limitation is observed (Fig. 8b). Finally, no more water can flow against the air stream (Fig. 8c) and the water is gradually pushed back towards the bend (Fig. 8). This results in the formation of swirls in the manifold. These phenomena were also observed in the experiment.

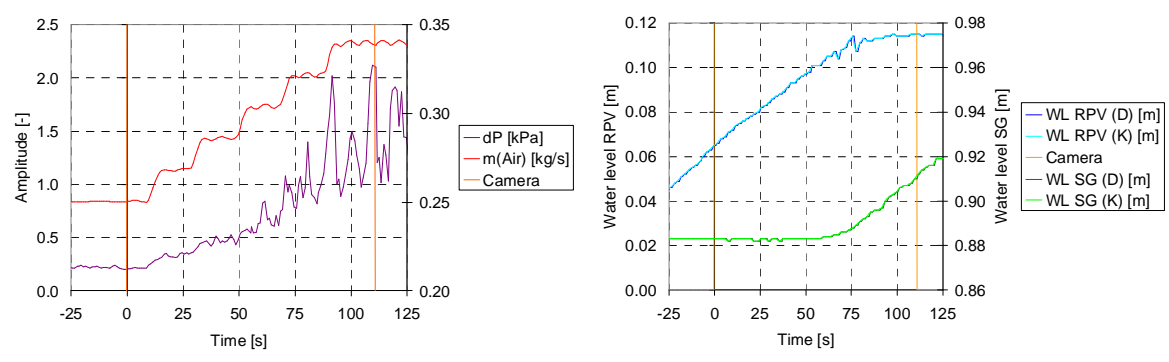


Fig. 7 Experiment 30-05 - used as a boundary condition data, left: air mass flow and pressure difference between the two separators, right: water levels

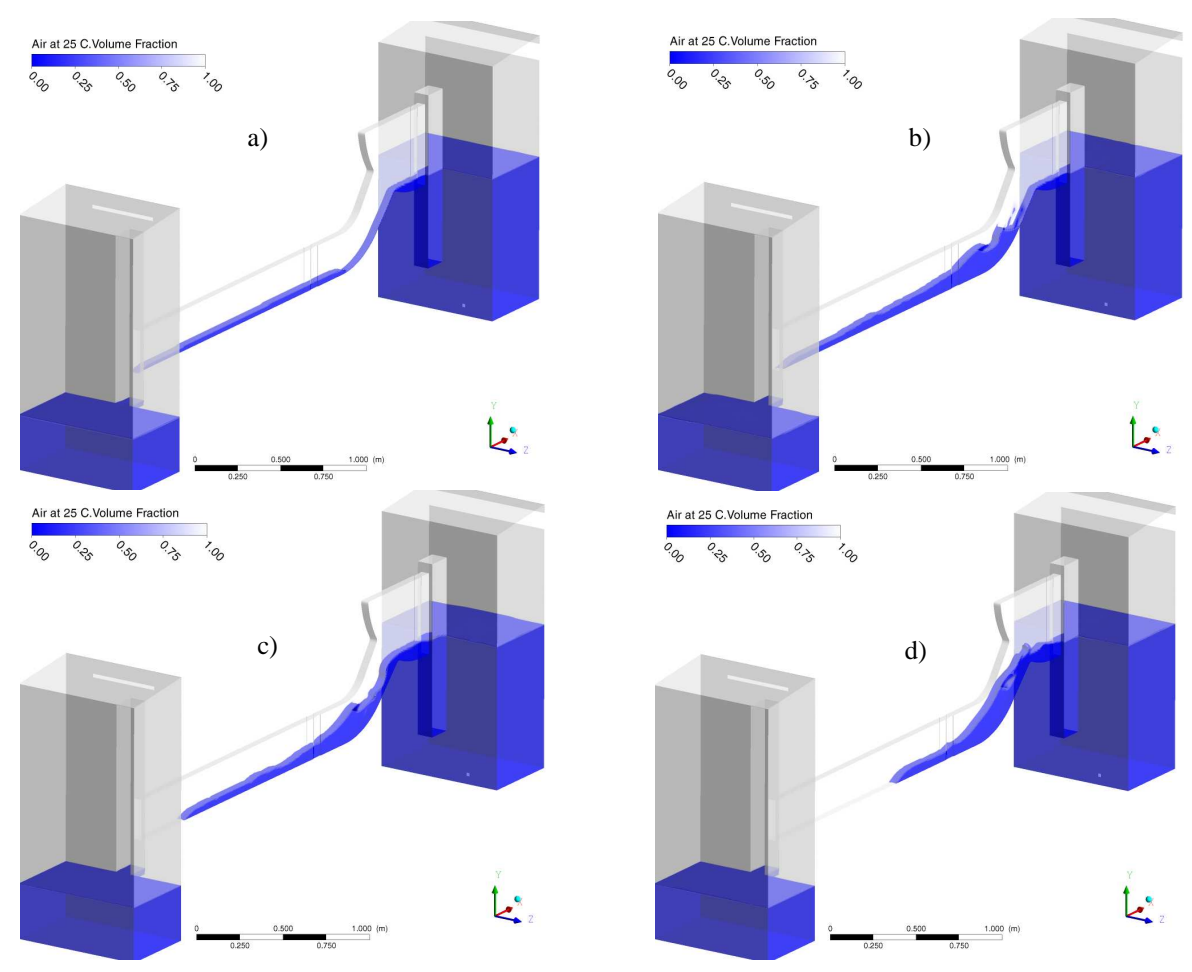


Fig. 8 Snapshots from the CFD simulation: a) counter-current flow without limitation, b) flow with partial counter-current limit, c) full counter-current limit, d) pushing back the water

Figures 9 to 12 give further qualitative flow phenomena of the CFD calculation in comparison with the experiment. Thus, in Fig. 9, a hydraulic jump at the channel is observed.

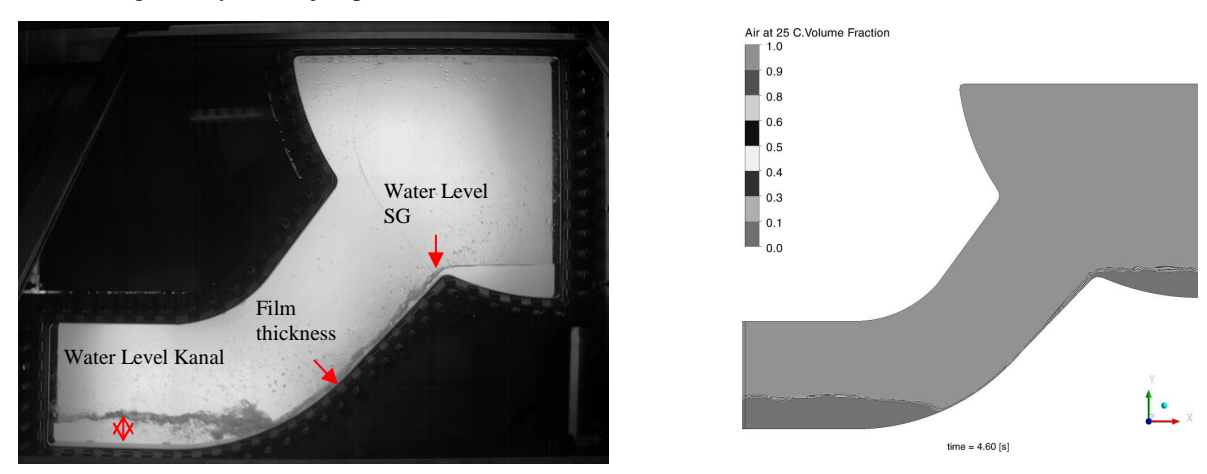


Fig. 9 Comparison of experiment and simulation for the flow before the onset of the counter-current flow limitation

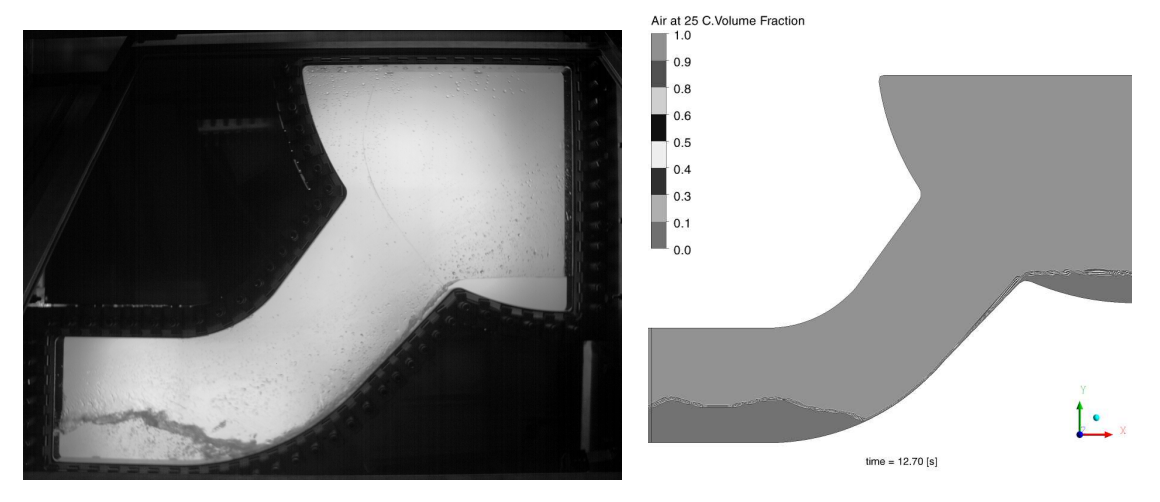


Fig. 10 Comparison of experiment and simulation for the flow at the start of wave formation

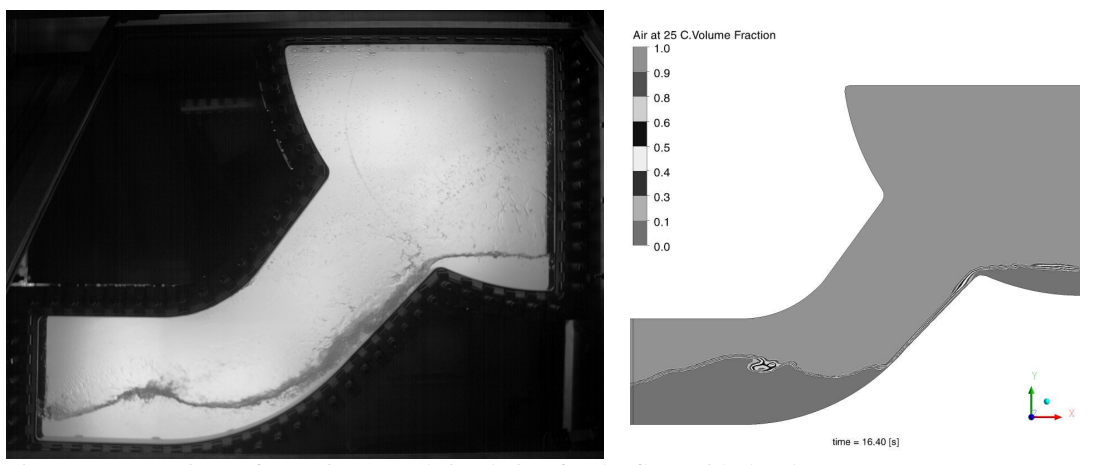


Fig. 11 Comparison of experiment and simulation for the flow with droplets

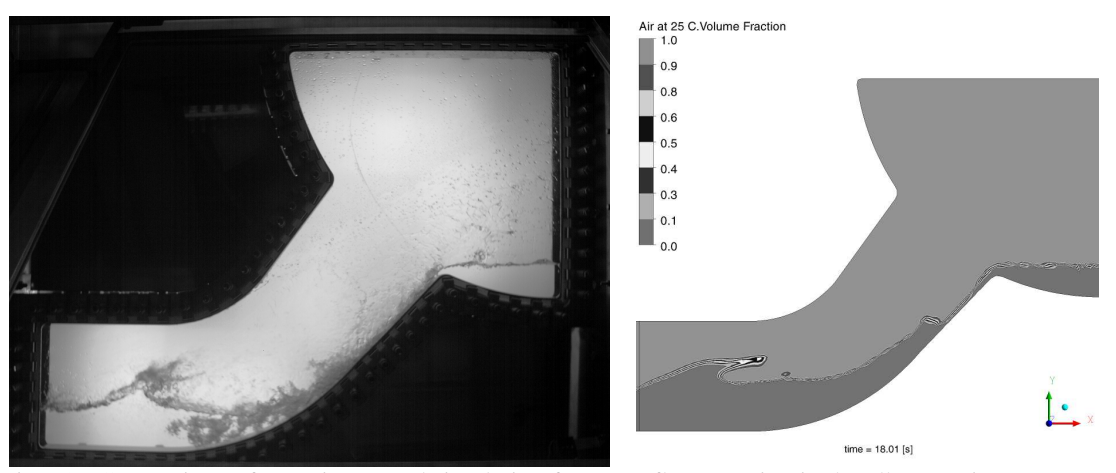


Fig. 12 Comparison of experiment and simulation for wavy flow, starting in the elbow region

In Fig. 10 similar wave formations can be seen. A drop can be seen in Fig. 11. Fig. 12 shows in both cases, a high migration of the crests of the waves towards the SG bottom, so that the down-running film disturbed.

The Table 2 is an attempt of a quantitative comparison of the water level in the channel, the film thickness in the elbow and the water level in the SG bottom (see Fig. 12). The quantitative agreement of calculations and measurements is quite good, especially with regard to water levels. Comparing the film thickness must be remembered that the video camera recorded the entire width including side walls, while the CFD calculation includes only a central section plane. Thus, the film thickness in the calculation is smaller.

Table. 2: Quantitative		

Quantitative comparison	Experiment	CFX
Water Level Channel:	26 mm	30 mm
Film thickness:	6,7 mm	3,4 mm
Water Level SG:	7 mm	7,5 mm

4.2 CCFL Experiments 30-09 (Air-Water) and 11-01 (Steam-Water)

Two additional calculations have been performed of two HZDR TOPFLOW Hot Leg experimental runs (30-09 and 11-01) to simulate the effect of fluid properties, and they are summarized in Table 1. The injected gas mass flow rates used in the present calculation were a function of time as shown in Fig. 13.

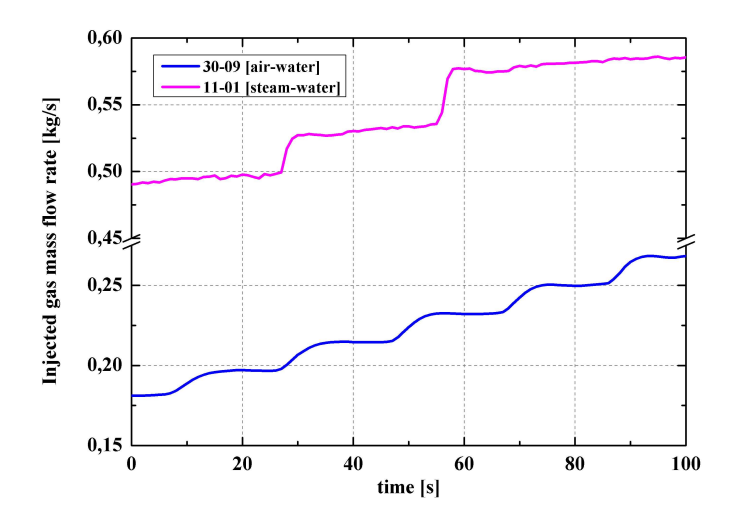


Fig. 13 Injected gas mass flow rate as a function of time of both calculation runs

Fig. 14 shows the calculated results of the average water level inside the RPV simulator and the experimental data of the stepwise increase of the injected air mass flow rate. The water level and injected air mass flow rate are shown by the blue and pink curves respectively. In the Fig. 14, (a), and (b) corresponds to the calculated water level of the steam-water and air-water respectively. From this figure, the phenomena can be explained as follows.

The water level characteristics of both cases are similar, and they are divided into three regions. In the first region, the water level in the RPV simulator increases with a constant slope as air mass flow rate increases. This region is defined as the stable counter-current flow region. In the second region, the slope of the curve of water level in the RPV simulator begins to decrease. This point is known as the onset of flooding or counter-current flow limitations. In the third region, the calculated water level shows a plateau. This means that all the injected water in SG separator do not flow to the side RPV simulator. This point is known as the zero liquid penetration. The region between the onset of flooding and zero liquid penetration is defined as the partial delivery region.

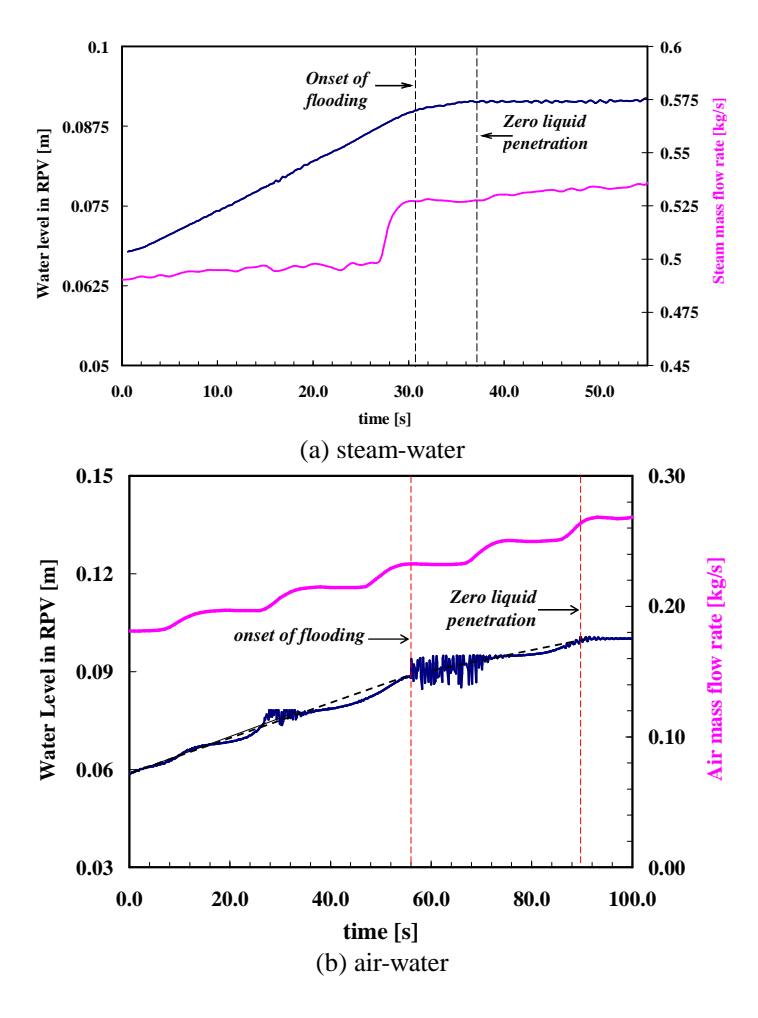


Fig. 14 Time variation of the calculated result of the water level in the RPV simulator (blue curve), and the experimental data of the injected gas mass flow rate (pink curve)

A comparison of the CCFL characteristics between the CFD calculation and experiment is shown in Fig. 15. For a meaningful comparison, the non-dimensional superficial velocity J_k^* , namely as Wallis parameter, is used to plot the CCFL characteristics. Here the Wallis parameter in Fig. 15 is defined as follows.

$$J_{k}^{*} = J_{k} \sqrt{\frac{1}{gH} \cdot \frac{\rho_{k}}{(\rho_{L} - \rho_{G})}}$$
 (14)

where H is the height of the channel. Close inspection of Fig. 15 reveals that the calculated CCFL points pass through the range of HZDR experimental data, indicating a good agreement between the calculation and experimental data. In comparison between both simulation results (11-01 & 30-09) indicates that there is a minor effect of the fluid viscosities on the zero liquid penetration point $((J_L^*)^{1/2}=0.0)$, and the fluid viscosities effect increases with the increase of $(J_L^*)^{1/2}$.

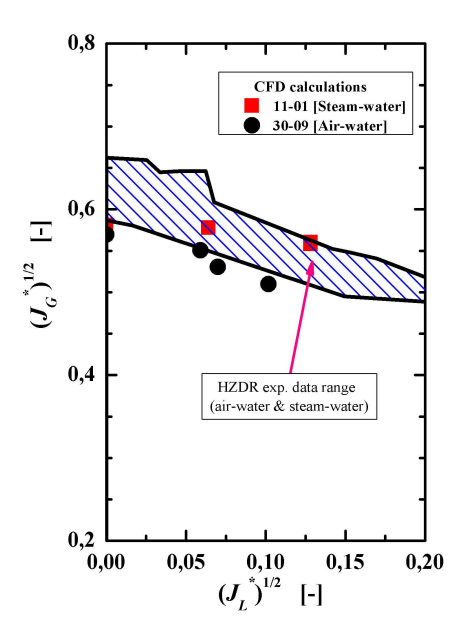


Fig.15 CCFL characteristics

In order to make a quantitative comparison on the water level inside the hot leg channel between the experiment and calculation, interface capture method was developed. To capture the gas-liquid interface in the camera frames, an image processing algorithm was developed. This technique allows the representation of the interface by a water level as a function of locus in the channel x and the time t. Nevertheless, for a comparison between the CFD calculation and experimental result, a surface similar to the interface in the camera pictures has been defined. Therefore an isosurface with a void fraction of 50 % was chosen and the coordinates of its intersection with the vertical mid-plane was exported from ANSYS CFX. With this simplification, the three-dimensional shape of the isosurface is not taken into the account.

The time-averaged water level profiles for both of experimental and CFD calculation is shown in Fig. 16 for air-water case. In the Figure, the water level data are presented as a function of location and the superficial gas velocity. Qualitatively, Fig. 16 shows that the trend obtained for the simulation is similar to the measurement. As in the experiment, before the onset of flooding the mean water level profile in the horizontal part increases as the distance far from the inclined part. However, a detailed comparison shows a little quantitative deviation between simulations and measurement. The possible reasons are the detected of the maximal value of the water level due to the three dimensional effect in the measurement or the inlet boundary condition. Therefore future works on those problems should be considered.

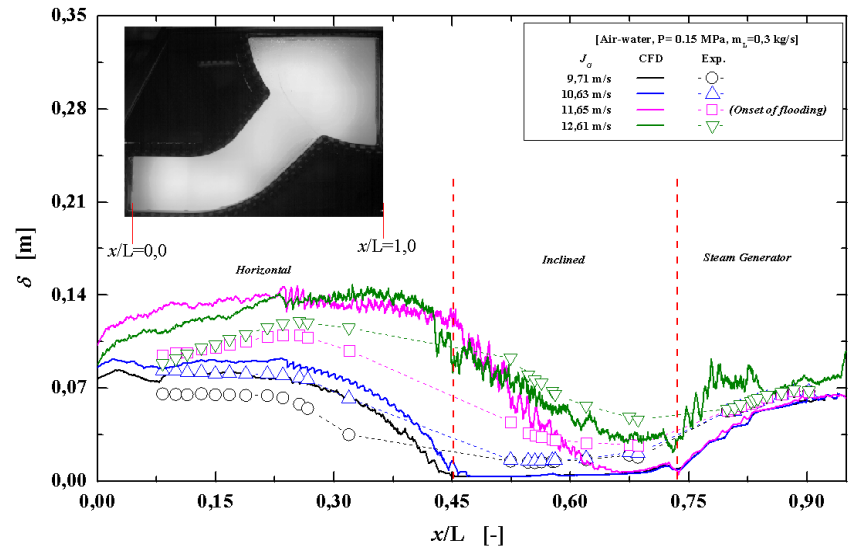


Fig. 16 The comparison on the water level inside the hot leg channel between experiment and CFD calculation (airwater test)

CONCLUSIONS

Three-dimensional CFD simulations of the CCFL phenomenon of gas-liquid two-phase flow in a model of hot leg a German Konvoi Pressurized Water Reactor with rectangular cross section have been performed using the Euler-Euler inhomogeneous mixture model. Selected air-water and steam-water CCFL experiments of HZDR TOPFLOW Hot Leg were chosen for transient CFD simulations. An Algebraic Interfacial Area Density (AIAD) model on the basis of the implemented mixture model was implemented. A picture sequence recorded during the CCFL experiment was compared with CFD simulation of the commercial code of ANSYS CFX 12.0. The calculated results of the velocity profile and water volume fraction indicate that the basic flow characteristics of the experiment such as the hydraulic jump near the bended region of the hot leg PWR and the occurrence of roll wave were reproduced in simulation. In addition, the calculated CCFL characteristics and water level inside hot leg channels points were also in an a good agreement with the experiments, while a minor deviation require a continuation of the work. The usage of the morphology detection algorithm AIAD should also be possible in vertical flow regimes. Therefore it is necessary to include the modelling of non-drag forces (lift force, wall lubrification force, virtual mass force etc.) as well as the MUlti bubbe SIze Group (MUSIG) model for polydispersed flows. Also the turbulence damping procedures should include the existence of small surface instabilities in the macroscopic model. Further the damping functions from the liquid side should be improved. The goal is to provide an easy usable AIAD framework for all users, with the possibility of the implementation of their own correlations.

ACKNOWLEDGEMENTS

This work is carried out within the frame work of a current research project funded by the German Federal Ministry of Economics and Technology, project number 150 1329. Dr. Deendarlianto is an Alexander von Humboldt Fellow in the Institute of Safety Research, Helmholtz-Zentrum Dresden-Rossendorf e.V., Germany.

NOMENCLATURE

- A Interfacial area density (m⁻¹)
- C_D Drag coefficient (-)
- d Diameter (m)
- F_D Interfacial friction force (N)
- f Blending function (-)
- g Gravitational constant (ms⁻¹)

- H Channel height (m)
- J_k^* Non dimensional superficial velocity by Wallis (-

- Void fraction (-)
- p Pressure (Nm⁻²)
- U Velocity (ms⁻¹)

Greek letters

- ρ Density (kg/m³)
- μ Dynamic viscosity (Pa.s)
- η Viscosity (Pas)
- τ Shear stress (N/m²)

Subsripts

- B Bubble
- D Droplet
- FS Free surface
- G Gas phase
- k Gas or Liquid phase
- L Liquid phase

REFERENCES

Ardron, K.H., et al., 1986, International Journal of Multiphase Flow, Vol. 12-4, pp. 543-558.

Bertadano, M.L., 1994, Nuclear Science and Engineering, Vol. 117, pp. 126-133.

Deendarlianto, et al., 2008, Nuclear Engineering and Design, Vol. 238-12, pp.3389-3402.

Geweke, M., et al., 1992, In: Proceeding of European Two-Phase Flow Group Meeting, Stockholm, June, Paper No. J1.

Höhne, T.; Vallée, C. 2010 The Journal of Computational Multiphase Flows 2(2010)3, 131-143

Höhne, T., and Vallée, C., 2009, In: Proceeding of the 13th International Topical Meeting on Nuclear Reactor Thermal Hydraulics (NURETH-13), Kanazawa, Japan.

Jeong, H.Y., 2002, Annals of Nuclear Energy, Vol. 29-5, pp. 571-583.

Kukita, et al., et al., 1987, In: Proceeding the Winter Annual meeting of the ASME, Boston, USA, 111-116.

Lee, S.C., and Bankoff, S.G., 1983, Journal of Heat Transfer, Vol. 105, pp. 713-718.

Menter, F.R., 1993, AIAA, Vol. 93,p. 2906.

Menter, F.R., 2002, ECORA FIKS-CT-2001-00154.

Ohnuki, A., 1986, Journal of Nuclear Science and Technology, vol. 23, pp. 219-232.

Prasser, H.M., et al., 2006, Kerntechnik, Vol. 71, pp. 163–173.

Vallée, C., et al., 2009, In: Proceeding of the 13th International Topical Meeting on Nuclear Reactor Thermal Hydraulics (NURETH-13), Kanazawa, Japan (2009)

Wang, M.J., and Mayinger, F., 1995, Nuclear Engineering and Design, Vol 155, pp. 643-652.

Wongwises, S., 1996, Nuclear Engineering and Design, Vol. 166-2, pp. 121-133.

Yegorov, Y., ,2004, EVOL-ECORA- D07 (2004).